Journal of Medicinal Chemistry

Article

pubs.acs.org/jmc

Discovery of Selective Phosphodiesterase 1 Inhibitors with Memory Enhancing Properties

Brian Dyck,*[,†] Bryan Branstetter,[†] Tawfik Gharbaoui,[†] Andrew R. Hudson,[†] J. Guy Breitenbucher,[†] Laurent Gomez,[†] Iriny Botrous,[†] Tami Marrone,[†] Richard Barido,[†] Charles K. Allerston,[†] E. Peder Cedervall,[†] Rui Xu,[†] Vandana Sridhar,[†] Ryan Barker,[†] Kathleen Aertgeerts,[†] Kara Schmelzer,[†] David Neul,[†] Dong Lee,[†] Mark Eben Massari,[†] Carsten B. Andersen,[†] Kristen Sebring,[†] Xianbo Zhou,[†] Robert Petroski,[†] James Limberis,[†] Martin Augustin,[§] Lawrence E. Chun,[‡] Thomas E. Edwards,[‡] Marco Peters,[†] and Ali Tabatabaei[†]

[†]Dart Neuroscience LLC, 12278 Scripps Summit Drive, San Diego, California 92131, United States

[‡]Berylllium, 7869 NE Day Road West, Bainbridge Island, Washington 98110, United States

[§]Proteros Biostructures GmbH, Bunsenstraße 7a, D-82152 Martinsried, Germany

Supporting Information

ABSTRACT: A series of potent thienotriazolopyrimidinone-based PDE1 inhibitors was discovered. X-ray crystal structures of example compounds from this series in complex with the catalytic domain of PDE1B and PDE10A were determined, allowing optimization of PDE1B potency and PDE selectivity. Reduction of hERG affinity led to greater than a 3000-fold selectivity for PDE1B over hERG. 6-(4-Methoxybenzyl)-9-((tetrahydro-2*H*-pyran-4-yl)methyl)-8,9,10,11-tetrahydropyrido[4′,3′:4,5]thieno[3,2-*e*][1,2,4]triazolo[1,5-*c*]pyrimidin-5(6*H*)-one was identified as an orally bioavailable and brain penetrating PDE1B enzyme inhibitor with potent memory-enhancing effects in a rat model of object recognition memory.

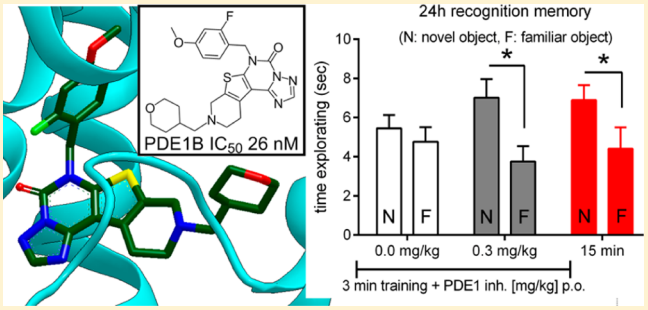

INTRODUCTION

Cognitive decline and loss of memory with age has a significant impact on daily functioning and quality of life.[1] These deficits are even more prominent in many neurodegenerative and psychiatric disorders such as depression, Alzheimer's disease, Huntington's disease, and schizophrenia. Plainly, there is a significant need for new drugs which ameliorate these cognitive deficits. Most drug discovery efforts to intervene in cognitive dysfunction have focused on neurotransmitter systems thought to be involved in cognitive functioning, including acetylcholine, serotonin, histamine, glutamate, and dopamine systems.[2] However, an alternative approach is to target enhancement of the downstream signaling cascades that result from activation of these neurotransmitter systems, which trigger activity-dependent gene expression and support long-lasting changes in synaptic structure and function.[3]

cAMP and cGMP are ubiquitous second messengers which are upregulated upon neuronal activation. Phosphodiesterases (PDEs) are the enzymes which hydrolyze, and thereby inactivate, these second messengers, making the PDEs essential for the termination of cGMP and cAMP signaling. Eleven families consisting of 21 mammalian genes encoding individual PDE isoforms have been identified.[4,5] Because of their critical role in signal transduction, PDEs are key molecular targets for therapeutic intervention in a variety of peripheral disorders. Among them, PDE5 inhibitors marketed for the treatment of erectile dysfunction and pulmonary artery hypertension have shown the most success (sildenafil, tadalafil, vardenafil). In addition, PDE4 inhibitors have been approved for the treatment of COPD and psoriasis (roflumilast, apremilast) and PDE3 inhibitors for acute treatment of congestive heart failure (milrinone).

Because of the putative impact of cAMP and cGMP on neuronal plasticity, PDE inhibitor have potential utility for CNS disorders.[6,7] The second messenger cAMP activates cAMP response element-binding protein (CREB) signaling via protein kinase A (PKA) and can thereby modulate transcription of genes associated with synaptic plasticity, such as brain-derived neurotrophic factor (BDNF).[8] This cAMP/PKA/CREB pathway has been implicated in the enhancement of long-term potentiation (LTP), which is considered the neurophysiological correlate of memory.[9−11]

Among the PDEs expressed in the CNS, the dual specificity PDE1B may play a unique role pertaining to memory.[12,13] Like PDE4 and PDE10, inhibition of PDE1B increases cAMP levels

Received: February 22, 2017

DOI: 10.1021/acs.jmedchem.7b00302
J. Med. Chem. XXXX, XXX, XXX−XXX

in the striatum.[12,14] PDE1 is coexpressed with dopamine receptors, as are PDE4 and PDE10, suggesting these PDEs are responsible for terminating the cAMP signal associated with dopaminergic activation. However, Nishi et al. have proposed PDE4 and PDE10 activate DA neurons predominantly via the indirect D2 pathway and PDE1B couples with the direct pathway via D1 signaling.[15] This offers an explanation why a PDE1B inhibitor reversed haloperidol-induced catalepsy in rats, whereas inhibitors of PDE4 and PDE10 enhance catalepsy induced by haloperidol.[16a] Consequently, a PDE1B inhibitor may be well suited to treat cognitive and motor deficits associated with deficient D1 dopaminergic signaling such as exists in Parkinson's disease.

Few selective PDE1 inhibitors have been disclosed thus far (Chart 1). Vinpocetine, a commonly used nutraceutical with

Chart 1. PDE1B Inhibitors

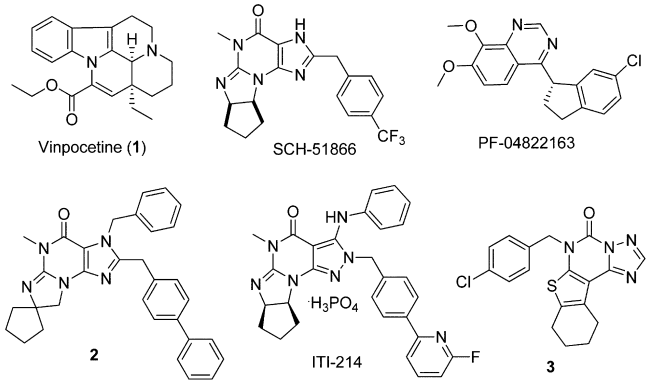

putative ameliorating effects on primary dementia, has minimal activity at PDE1B in our hands.[17] The modest PDE1 potency and off-target activity of this compound suggest that experiments using vinpocetine to determine PDE1 pharmacology should be interpreted with caution. Other potent PDE1 inhibitors have been reported with cross-reactivity with PDE5, PDE9, and PDE10.[18−22] Scientists from Schering-Plough have optimized the dual PDE1/PDE5 inhibitor SCH-51866 (PDE1 IC_{50} 0.070 μM, PDE5 IC_{50} 0.060 μM) to compounds with greater than 300-fold selectivity for PDE1 over PDE5 (e.g., **2**).[19,23] Intra-Cellular Therapies has identified potent PDE1 inhibiting pyrazolopyrimidinones structurally related to the Schering-Plough imidazopyrimidinones.[16] One example (**ITI-214**, PDE1B IC_{50} 0.000058 μM) demonstrated efficacy in a rat novel object recognition (NOR) task at 1 and 3 mg/kg (PO), and has advanced into the clinic in partnership with Takeda.[24] Recently, scientists from Pfizer have also disclosed a brain-penetrating quinazoline-based PDE1 inhibitor **PF-04822163** (PDE1B IC_{50} 0.0024 μM), but no efficacy data was reported.[25]

RESULTS AND DISCUSSION

Screening our compound collection for PDE1B inhibitory activity generated the triazolopyrimidinone lead **3**. Despite cross-reactivity with several PDEs, including cGMP-specific PDE5 and PDE6, the low molecular weight and polar surface area of **3** suggested it may make a suitable scaffold for optimization (Table 2). Attempts to model **3** within the published apo PDE1B structure (accession code 1TAZ) were unsuccessful, so a crystal structure of this compound bound to the catalytic domain of PDE1B was determined (Figure 1).[26]

The reason for the difficulty encountered while trying to model **3** within the ligand-free PDE1B structure became clear upon obtaining a crystal structure of the complex. The carbonyl of compound **3** forms hydrogen bonds with the side chain of Gln421 and His373, and there is a favorable interaction between the triazole nitrogen N(1) and the side chain of His373. This orientation of the ligand places the 4-chlorobenzyl group into a newly formed lipophilic pocket which arises from a rotation of Met389 relative to the apo structure of the protein. Phe424 and Leu388 form the hydrophobic clamp typical of PDE structures. The cyclohexyl ring of **3** protrudes into a solvent exposed region, which we thought to exploit to optimize physicochemical properties of the compound and perhaps impart additional selectivity over other PDEs. One option we felt was attractive was to use a fused piperidine ring in replacement of the cyclohexyl group due to its higher water solubility and chemical versatility.

The synthetic route used to prepare the piperidinothiophene analogues of **3** is shown in Scheme 1. Reaction of protected piperidinones **4** and **5** with elemental sulfur and malonitrile under the conditions described by Wang and co-workers afforded **6** and **7**.[27] These were converted to the ethyl carbamates and heated with formylhydrazine to afford tectracyclics **8** and **9**.[28] Substituted benzyl groups were introduced by *N*-alkylation and the *t*-butoxycarbonyl group was removed by the action of trifluoroacetic acid, yielding piperidines **10**−**15**. Substitution on the piperidine nitrogen atom was accomplished by reductive alkylation with an

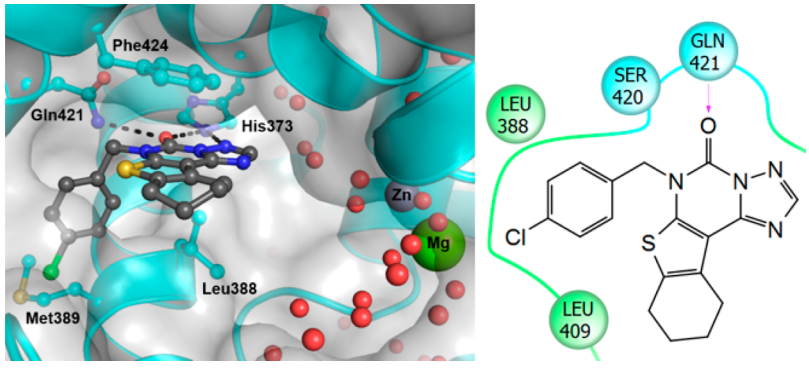

Figure 1. Crystal structure of **3** bound to the catalytic domain of PDE1B and ligand interaction guide. Key residues are labeled, including the hydrophobic clamp (Phe424 and Leu388).

DOI: 10.1021/acs.jmedchem.7b00302
J. Med. Chem. XXXX, XXX, XXX−XXX

Scheme 1. Synthesis of Thienopyrimidinone PDE1 Inhibitors[a]

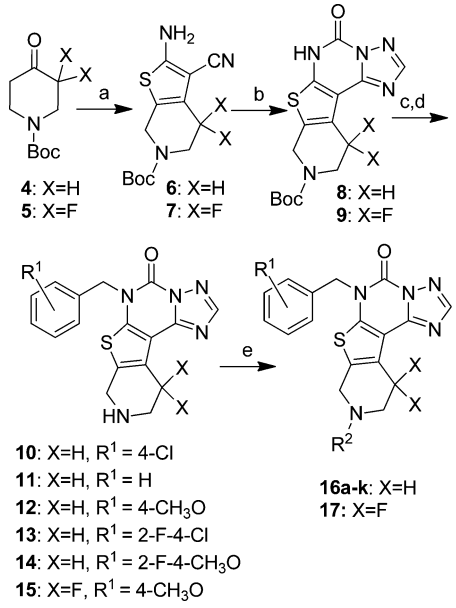

[a]Reagents and conditions: (a) malonitrile, sulfur, proline, DMF, 60 °C; (b) ethyl chloroformate, pyridine, DCM, then formyl hydrazine, DIEA, DMA, 150 °C; (c) $ArCH_2Cl$, K_2CO_3, DMF, 60 °C; (d) TFA, DCM; (e) aldehyde/ketone, $NaBH(OAc)_3$, DCE or cyclopropylcarbonyl chloride, TEA, DCM or 2,2-difluorocyclopropanecarboxylic acid, TEA, HOBt, EDC, DCM.

aldehyde or ketone or acylation under standard conditions, thereby affording target compounds **16a–k** and **17**.

The activity of the piperidines **16a–k** and **17** at PDE1B is shown in Table 1, along with in vitro microsomal stability data and inhibitory data against two antitargets, PDE10 and hERG. As predicted by the crystal structure shown in Figure 1, substitution of nitrogen for carbon in the cyclohexyl ring did not negatively influence PDE1B activity, as **3** and **16a** exhibit similar potency at PDE1B. We did however observe a substantial increase of potency at the hERG channel, which may not have been unexpected with the addition of a tertiary amine functionality. Substitution of the nitrogen atom with cyclopropylmethyl (**16b**) resulted in a 5-fold increase in potency at PDE1B and a modest improvement in hERG activity. Rendering the molecule nonbasic by introducing an amide functionality into **16c** increased the potency 4-fold at PDE1B relative to **16b** and reduced the hERG potency by 3-fold. Unfortunately, acyl substituted piperidines consistently inhibited PDE10A. In fact, this PDE10 activity was optimized to produce potent dual PDE1/PDE10 inhibitors such as **16d**. In an effort to understand the origin of the cross-reactivity with PDE10, we determined a crystal structure of the complex of **16d** with the catalytic domain of PDE10A (Figure 2).

The binding mode of **16d** in PDE10A is inverted relative to that of similar compounds bound to PDE1B. A triazole nitrogen atom forms a hydrogen bond with the conserved glutamine (Gln726). The hydrophobic clamp of PDE10A (Phe729 and Ile692) encloses the tetracyclic core, and the carboxamide side chain extends distally from the metal centers. From the PDE10 crystal structure, it is difficult to ascertain why the compounds containing a carboxamide functionality are consistently more potent at PDE10 than the corresponding amines. This portion of the inhibitor does occupy a narrow (and lipophilic) channel formed by Phe729 and Met713. The pK_a of **16j** was determined experimentally to be 6.6, so a significant fraction of the aminergic inhibitors would be expected to be protonated at physiological pH. It is possible the narrow, lipophilic channel does not tolerate ionized groups. In any case, a basic nitrogen atom at this site proved to be a good approach to achieve selectivity over PDE10.

In terms of PDE1B inhibition, alkyl (**16b**), benzyl (**16f**), and cyclic ether-substitution (**16e** and **16h**) all provided potent examples, but minimizing hERG activity while retaining a basic nitrogen within the piperidine ring proved challenging. A 4-substituted benzyl group on the pyrimidinone nitrogen atom improved activity at PDE1B as **16g** was less potent, and fortunately modifications did allow attenuation of hERG activity. Replacement of the 4-chloro group with a 4-methoxy as in **16j** led to a 6-fold reduction in hERG potency. An additional ortho substituent on the benzyl ring as in **16i** and **16k** had a modest positive effect on hERG activity as well, but the ratio of hERG IC_{50} to PDE1B IC_{50} remained largely unchanged at 80-fold. A two log reduction of the pK_a of the piperidine nitrogen atom by β-difluorination as in **17** resulted in a 9-fold improvement in PDE1B potency and a 4-fold increase in the hERG IC_{50}. Consequently, **17** exhibited greater than a 3000-fold ratio between its PDE1B IC_{50} and hERG IC_{50}.

Because of the modest hERG inhibition observed for these compounds, representatives were tested in anesthetized guinea pigs for signs of QT prolongation. No QT prolongation was observed for **16k** or **17** up to doses of 10 mg/kg IV (Figure 3). This suggests that the 80-fold ratio between in vitro hERG and PDE1 activities is probably sufficient to provide a safe margin in vivo (see efficacy doses below). Unfortunately, difluoropiperidine **17** was a substrate of MDR1 (P-gp) in MDCK cells with an efflux ratio greater than five, thereby precluding it from advancing as a candidate for CNS indications.

A crystal structure of **16j** with the catalytic domain of PDE1B was determined and the binding mode is similar to that of the screening hit **3** (Figure 4). The tetrahydropyranylmethyl group of **16j** protrudes into a pocket comprised of Leu409, Pro408, Phe392, and Thr271. It should be noted that the position of the tetrahydropyranylmethyl group could potentially be influenced by a second molecule of **16j** that is bound between two crystal symmetry related protein molecules, next to the active site of the PDE1B molecule in the asymmetric unit (see Supporting Information, Figure S1)

By improving PDE1B potency, the tetrahydropyranylmethyl group of **16k** imparted good selectivity with regard to other PDE families (Table 2). This is especially evident for the PDE6 isoform, in which the IC_{50} ratio for **16k** shows more than a 200-fold improvement relative to **3**. PDE6 expression is largely limited to the human retina and inhibition of this enzyme may be responsible for some of the visual side effects of marketed erectile dysfunction drugs.[29]

For the most part, the thienotriazolopyrimidinones were stable in human and rat liver microsomes (Table 1). The exceptions were the methyl and cyclopropyl substituted piperidines **16a** and **16b** which were rapidly cleared in the microsomes from both species and benzyl substituted **16f**, which had moderate stability in human microsomes, but not rat microsomes. Fortunately, **16k** had good stability in the in vitro assay for both species and is not a P-gp substrate (MDCK efflux ration = 1.0). Hence, the compound was evaluated in rats orally and intravenously (Figure 5).

DOI: 10.1021/acs.jmedchem.7b00302
J. Med. Chem. XXXX, XXX, XXX−XXX

Table 1. In Vitro Properties of Key Compounds

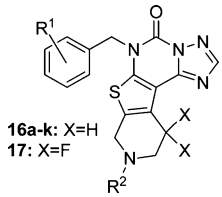

Cmpd	R^1	R^2	PDE1B IC_{50} (μM)[a]	PDE10A IC_{50} (μM)[a]	hERG IC_{50} (μM)[a]	HLM (μL/min/mg)[b]	RLM (μL/min/mg)[c]
1	-	-	>10	>10	0.039	N.D.	N.D.
2	-	-	0.048	>10	>10	N.D.	N.D.
3	-	-	0.46	3.5	6.3	N.D.	N.D.
16a	4-Cl	CH3	1.0	>10	0.069	>300	>300
16b	4-Cl		0.21	>10	0.16	118	>300
16c	4-Cl		0.053	1.2	0.49	6.0	23
16d	4-CH_3O		0.011	0.059	4.9	7.2	26
16e	4-Cl		0.15	>10	0.98	6.1	20
16f	4-Cl		0.19	>10	0.49	21	138
16g	H		0.15	>10	0.57	14	0
16h	4-Cl		0.041	>10	0.35	9.0	18
16i	4-Cl-2-F		0.031	>10	0.61	10	21
16j	4-CH_3O		0.027	1.6	2.2	10	20
16k	4-CH_3O-2-F		0.026	0.69	2.7	11	22
17	4-CH_3O		0.003	1.7	9.2	6.7	8.5

[a]Values are averaged from a minimum of three replicates. Standard error of the mean (SEM) values were typically less than 40%. [b]Intrinsic in vitro clearance determined in human liver microsomes (HLM) in the presence of NADPH. [c]Intrinsic in vitro clearance determined in rat liver microsomes (RLM) in the presence of NADPH.

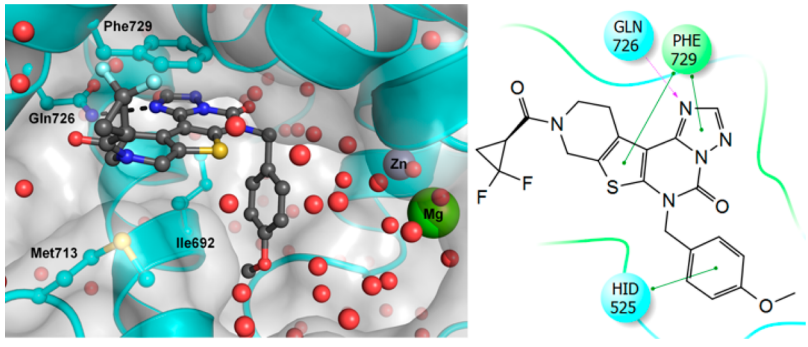

Figure 2. Crystal structure of **16d** bound to PDE10A and ligand interaction guide. Key residues are labeled, including the hydrophobic clamp (Phe729 and Ile692). HID, δ histidine.

DOI: 10.1021/acs.jmedchem.7b00302
J. Med. Chem. XXXX, XXX, XXX−XXX

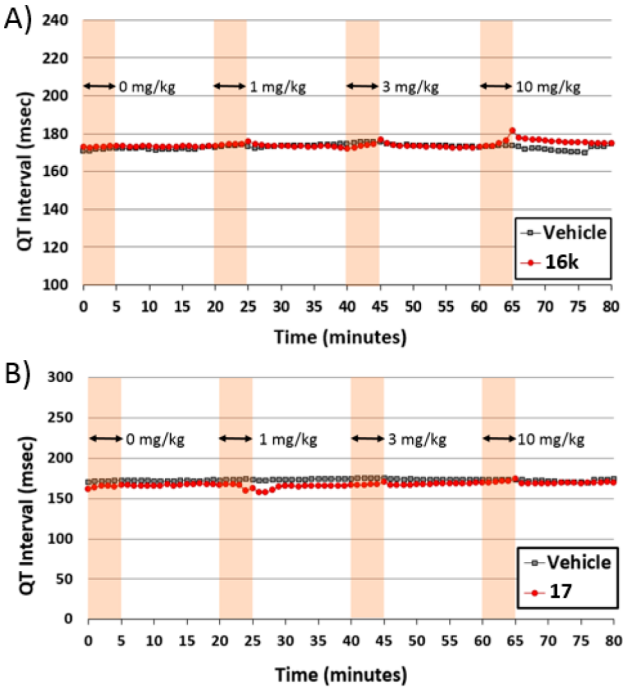

Figure 3. Effect of PDE1 inhibitors **16k** and **17** on the QT interval of anesthetized guinea pigs. (A) **16k** infused at 0, 1, 3, and 10 mg/kg (IV). (B) **17** infused at 0, 1, 3, and 10 mg/kg (IV).

Pharmacokinetic properties of **16k** were evaluated in male SD rats (200−250 g) following administration of a single 1 mg/kg IV or 5 mg/kg PO dose formulated as a solution in a mixture of NMP:PEG400:water (10:40:50). The compound was characterized as having a high volume of distribution (V_{ss}) and a moderate systemic clearance (50% of liver blood flow). The elimination half-life was determined to be 2.3 h. Following oral administration, **16k** was rapidly absorbed with a T_{max} of 0.8 h. It was found to be orally bioavailable (F = 90%) in rats and penetrate the brain ($B/P_{c,max}$ = 1.7). Compound **16k** was 1.6% unbound in rat brain tissue and 7.2% unbound in rat plasma. On the basis of this data, the compound was evaluated in a test of rat novel object recognition (NOR, Figure 6), a benchmark test of recognition memory in rodents.[30] In this paradigm, rats were allowed to explore two identical objects in the training phase. In the testing period, 24 h later, the rats were presented with one of the objects encountered during training (the familiar object) and a novel object. The natural curiosity of the animal caused it to spend more time exploring the new object. Measurement of the time spent with this novel object at the expense of the familiar object allowed one to quantify memory of the latter. A drug that improves memory should ideally augment performance of rats given suboptimal training to a

Table 2. PDE Selectivity Data for 3 and 16k

	compd **3**		compd **16k**	
	IC_{50} [a,b] (μM)	PDE1B selectivity	IC_{50} [a,b] (μM)	PDE1B selectivity
PDE1B	0.46	1	0.026	1
PDE2A1	4.1	9	7.9	>200
PDE3A	>10	>20	>10	>200
PDE4D3	3.9	8	9.3	>200
PDE5A	0.37	1	0.26	10
PDE6C	0.46	1	>10	>200
PDE7A1	>10	>20	>10	>200
PDE8A1	>10	>20	8.4	>200
PDE9A2	>10	>20	>10	>200
PDE10A1	4.0	9	0.74	29
PDE11A4	2.3	5	0.28	11

[a]PDE1B, PDE2A1, PDE3A, PDE4D3, and PDE10A1 IC_{50} values are averaged from a minimum of three replicates. Standard error of the mean (SEM) is typically less than 40%. [b]PDE5A, PDE6C, PDE7A1, PDE8A1, PDE9A2, and PDE11A4 IC_{50} values were determined at BPS Bioscience.

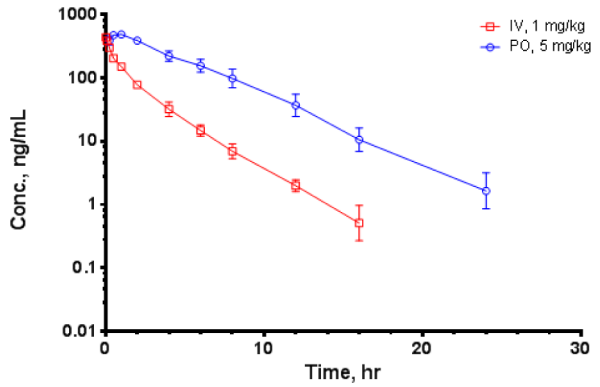

Figure 5. Rat plasma concentrations of **16k** following either a single 5 mg/kg PO or 1 mg/kg IV administration in 10:40:50 NMP:PEG400:-water.

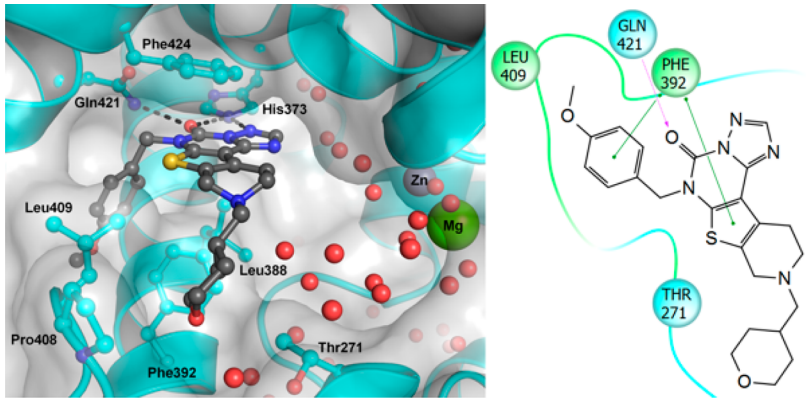

Figure 4. Crystal structure of **16j** bound to the catalytic domain of PDE1B and ligand interaction guide. Key residues are labeled, including the hydrophobic clamp (Phe424 and Leu388). The carbonyl group and N(1) of compound **3** form a hydrogen bond network with His373 and Gln421.

DOI: 10.1021/acs.jmedchem.7b00302
J. Med. Chem. XXXX, XXX, XXX−XXX

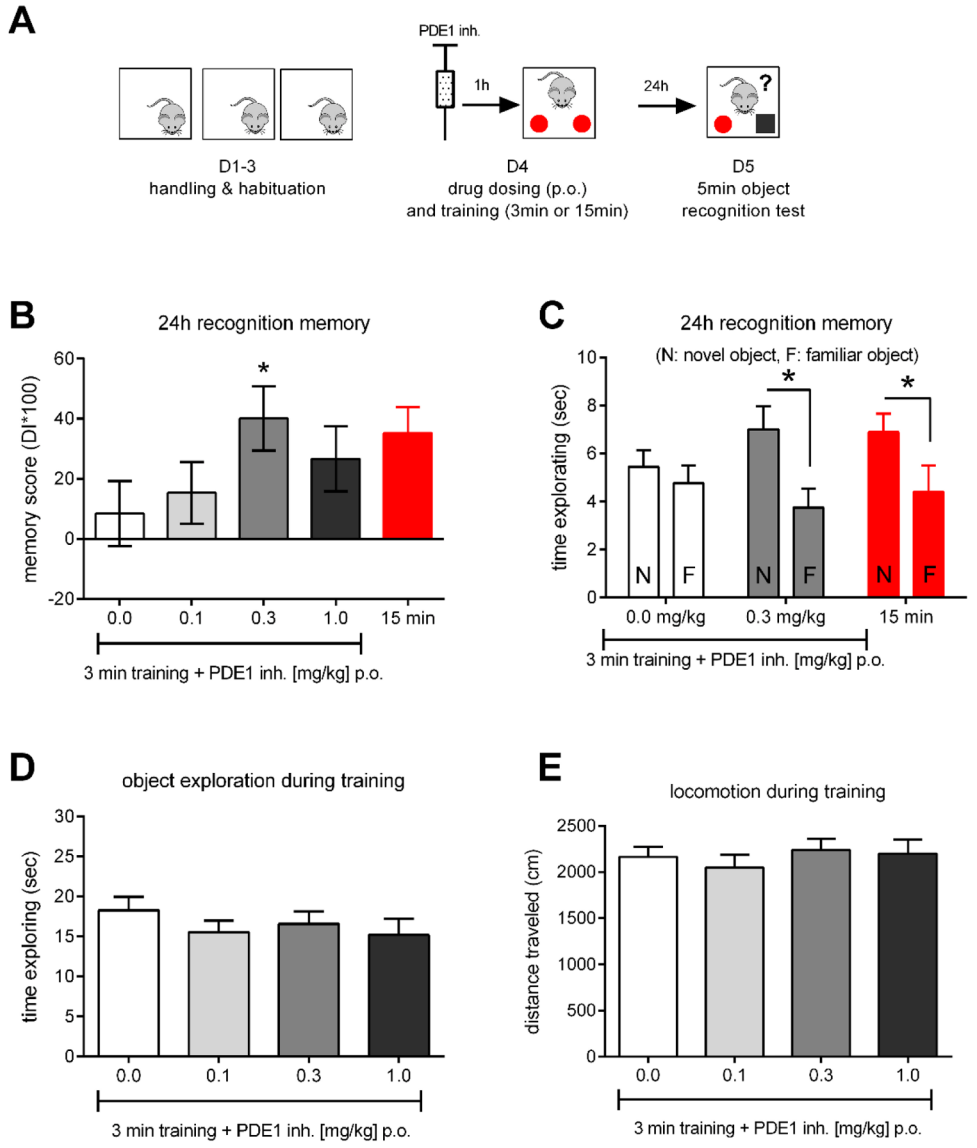

Figure 6. Effect of **16k** in a rat model of recognition memory. (A) Experimental procedure. Rats were habituated for 3 days. On day four, vehicle or drug was given and the rats trained for 3 min to induce a weak memory against which a drug effect could be measured. A separate group of rats was treated with vehicle and trained for 15 min as a performance control. (B) Effect on 24 h memory retention. Rats treated with 0.3 mg/kg **16k** showed significantly stronger memory for the familiar object than rats treated with vehicle and trained for 3 min. Memory in this group was comparable to the 15 min training + vehicle control. *$p < 0.05$ vs vehicle. (C) Effect of drug on exploration of the novel and familiar object during memory testing. Rats treated with 0.3 mg/kg **16k**, but not vehicle treated rats, spent significantly more time exploring the novel object. *$p < 0.05$ for novel vs familiar. (D) **16k** did not affect object exploration during training. (E) **16k** did not affect locomotion during training. All groups $N = 18–22$. The mean ± SEM are shown.

comparable level as untreated animals trained to induce a strong memory (i.e., more exposure to objects during the training phase). Studies in monkeys and rodents indicate that the hippocampus and cortical structures are important for recognition memory, and both areas show high levels of PDE1 expression.[31−36] We dosed rats orally with **16k** or vehicle 60 min prior to training and trained for 3 min to induce a weak memory for the trained object (Figure 6A). Rats treated with 0.3 mg/kg **16k** showed significantly enhanced recognition memory compared to vehicle treated rats in a retention test given 24 h later ($p < 0.05$, Figure 6B). At this dose, the maximum brain and free brain concentrations are estimated to be 110 and 1.8 nM, respectively. Memory in 0.3 mg/kg **16k** treated rats was comparable in magnitude to that observed in rats treated with vehicle and trained for 15 min (strong training), and both groups spent significantly more time exploring the novel object on test whereas vehicle treated rats trained for 3 min did not (Figure 6C). Importantly, **16k** did not affect the time exploring the objects or locomotion in the training phase, indicating that the drug did not alter exploratory behavior in rats (Figure 6D/E).

CONCLUSION

cAMP signaling is fundamental to memory formation. A number of access points to this important second messenger may be susceptible to pharmacological intervention, and phosphodiesterase inhibition is among the most studied. We have identified a series of selective PDE1 inhibitors with good pharmacokinetic properties and brain penetration to test memory effects in rats. Among these inhibitors, **16k** (**DNS-**

DOI: 10.1021/acs.jmedchem.7b00302
J. Med. Chem. XXXX, XXX, XXX−XXX

0056) increases long-term memory in a rat model of recognition memory, at brain concentrations near the PDE1B IC_{50}.[37] This compound shows potential as a tool to further probe the pharmacology of PDE1 inhibition. Moreover, related PDE1 inhibitors have promise as therapeutics to treat memory deficits and other conditions secondary to aberrant dopaminergic signaling.

EXPERIMENTAL SECTION

General Methods. Solvents and reagents were purchased and used without further purification unless otherwise noted. Vinpocetine (**1**) was purchased from Sigma-Aldrich. Compounds **2** and **6** were prepared as previously described.[19,27] Flash column chromatography (FCC) was performed on Teledyne Isco CombiFlash instruments equipped with silica gel columns. Preparative HPLC purification was performed on a Shimadzu Prominence system equipped with a Waters Sunfire OBD C18 5 μM 30 mm × 100 mm column. Elution was achieved with increasing concentration of acetonitrile in water and 0.05% trifluoroacetic acid added as modifier. Analytical HPLC was performed on an Acquity UPLC system equipped with a BEH C18 1.7 μM 2.1 mm × 50 mm column. Elution was achieved with increasing concentration of acetonitrile in water and 0.1% formic acid added as modifier. NMR was performed on a Bruker Ultrashield 400 Plus spectrometer. All final compounds gave satisfactory results (±0.4%) upon combustion analysis at Robertson Microlit Laboratories. QT prolongation studies in anaesthetized guinea pigs was performed by CorDynamics.

*tert-Butyl 2-Amino-3-cyano-4,4-difluoro-4,5-dihydrothieno[2,3-c]pyridine-6(7H)-carboxylate (**7**).* *tert*-Butyl 3,3-difluoro-4-oxopiperidine-1-carboxylate (5.10 g, 20 mmol), malononitrile (1.46 g, 22 mmol), sulfur (0.97 g, 30 mmol), and DL-proline (0.23 g, 2.0 mmol) were combined in DMF (25 mL) and heated at 65 °C for 18 h. The mixture was concentrated under vacuum and purified by FCC (elution with 10−80% ethyl acetate in hexanes) to afford 2.22 g (35%) of **7** as a yellow oil which solidified on standing. ^{1}H NMR (400 MHz, $CDCl_3$) δ 4.47 (br s, 2H), 4.13 (q, J = 7.11 Hz, 1H), 3.98 (t, J = 10.54 Hz, 2H), 1.45−1.53 (m, 9H), 1.26 (t, J = 7.15 Hz, 1H).

*tert-Butyl 5-Oxo-5,6,10,11-tetrahydropyrido[4′,3′:4,5]thieno[3,2-e][1,2,4]triazolo[1,5-c]pyrimidine-9(8H)-carboxylate (**8**).* General method A: Ethyl chloroformate (13.9 mL, 145 mmol) and pyridine (17.6 mL, 218 mmol) were added to an ice-cooled, stirred mixture of **6** (20 g, 73 mmol) in 1,2-dichloroethane (300 mL). After the addition was complete, the cooling bath was removed and the mixture was stirred for 5 h at room temperature. LCMS of the crude mixture indicated a mixture of the mono- and bis-ethoxycarbonylated products. The mixture was poured over water (300 mL) and extracted twice with DCM. The organic layers were combined, dried ($MgSO_4$), and concentrated under reduced pressure. The residue was diluted with methanol (300 mL) and water (15 mL) and treated with K_2CO_3 (5.0 g, 36 mmol). The resulting mixture was stirred at room temperature for 1 h, during which time the bis-ethoxycarbonylated material was converted to the desired monoethoxycarbonylated product. The mixture was poured over water (500 mL), and the desired product was extracted twice with DCM. The organic layers were combined, dried ($MgSO_4$), and concentrated under reduced pressure to yield 25 g (98%) of *tert*-butyl 3-cyano-2-((ethoxycarbonyl)amino)-4,5-dihydrothieno[2,3-*c*]pyridine-6(7*H*)-carboxylate as a brown solid, which was used in the following step without further purification.

DIEA (0.29 mL, 1.7 mmol) was added to a mixture of the above material (1.17 g, 3.33 mmol) and formic hydrazide (240 mg, 4.0 mmol) in DMA (14 mL), and the mixture was heated at 125 °C for 18 h. The mixture was cooled to room temperature and poured over a mixture of water (150 mL) and brine (100 mL). It was extracted six times with ethyl acetate, and the combined extracts were dried ($MgSO_4$) and concentrated. Residual DMA was present, so the material precipitated from ethyl acetate−hexanes and the resulting solid was isolated by filtration and air-dried to afford 475 mg (41%) of **8**. ^{1}H NMR (400 MHz, DMSO-d_6) δ 8.44 (s, 1H), 4.59 (s, 2H), 3.70 (t, J = 5.65 Hz, 2H), 2.93−3.02 (m, 2H), 1.45 (s, 9H). LCMS (MH+, 348.2).

*tert-Butyl 11,11-Difluoro-5-oxo-5,6,10,11-tetrahydropyrido-[4′,3′:4,5]thieno[3,2-e][1,2,4]triazolo[1,5-c]pyrimidine-9(8H)-carboxylate (**9**).* The title compound was prepared using general method A. ^{1}H NMR (400 MHz, DMSO-d_6) δ 8.53 (s, 1H), 7.39 (d, J = 8.53 Hz, 2H), 6.94 (d, J = 8.53 Hz, 2H), 5.37 (s, 2H), 4.74 (br s, 2H), 4.05−4.18 (m, 2H), 3.75 (s, 3H), 1.43 (s, 9H). LCMS (MH+, 504.2).

*6-(4-Chlorobenzyl)-5-oxo-5,6,8,9,10,11-hexahydropyrido-[4′,3′:4,5]thieno[3,2-e][1,2,4]triazolo[1,5-c]pyrimidin-9-ium 2,2,2-trifluoroacetate (**10**).* General method B: Potassium carbonate (1.59 g, 11.5 mmol) was added to a mixture of **8** (2.00 g, 5.76 mmol) and 4-chlorobenzyl chloride (1.11 g, 6.91 mmol) in DMF (20 mL). The resulting mixture was heated to 55 °C for 20 h, cooled to room temperature, and poured into water (200 mL) with vigorous stirring. The resulting precipitate was isolated by filtration and air-dried to afford 2.40 g (88%) of 6-(4-chlorobenzyl)-5-oxo-5,6,10,11-tetrahydropyrido[4′,3′:4,5]thieno[3,2-*e*][1,2,4]triazolo[1,5-*c*]-pyrimidine-9(8*H*)-carboxylate as an off-white powder. ^{1}H NMR (400 MHz, $CDCl_3$) δ 8.32 (s, 1 H), 7.41−7.45 (m, 1H), 7.34−7.37 (m, 2H), 5.39 (s, 2H), 5.39 (s, 2H), 4.59−4.69 (m, 2H), 3.74−3.82 (m, 2H), 3.11−3.21 (m, 2H), 1.51 (s, 9H). LCMS (MH+, 472.1).

The above material (1.70 g, 3.6 mmol) was dissolved in DCM (20 mL) and treated with TFA (5 mL). The resulting mixture was stirred at room temperature for 3 h, and it was concentrated under reduced pressure to yield **10** (1.68 g, 96%) as the trifluoroacetic acid salt. ^{1}H NMR (400 MHz, DMSO-d_6) δ 9.28 (br s, 2H), 8.55 (s, 1H), 7.44 (d, J = 2.76 Hz, 4H), 5.42 (s, 2H), 4.36 (br s, 2H), 3.43−3.55 (m, 2H), 3.16−3.26 (m, 2H). LCMS (MH+, 372.1).

*6-(Benzyl)-8,9,10,11-tetrahydropyrido[4′,3′:4,5]thieno[3,2-e]-[1,2,4]triazolo[1,5-c]pyrimidin-5(6H)-one Trifluoroacetate (**11**).* The title compound was prepared using general method B. ^{1}H NMR (400 MHz, DMSO-d_6) δ 9.28 (br s, 2H), 8.55 (s, 1H), 7.44−7.30 (m, 5H), 5.42 (s, 2H), 4.35 (s, 2H), 3.49 (t, J = 5.9 Hz, 2H), 3.21 (t, J = 5.6 Hz, 2H). LCMS (MH+, 338.1).

*6-(4-Methoxybenzyl)-8,9,10,11-tetrahydropyrido[4′,3′:4,5]thieno-[3,2-e][1,2,4]triazolo[1,5-c]pyrimidin-5(6H)-one Trifluoroacetate (**12**).* The title compound was prepared using general method B. ^{1}H NMR (400 MHz, DMSO-d_6) δ 9.22−9.29 (m, 1H), 8.53 (s, 1H), 7.32−7.42 (m, 2H), 6.94 (s, 2H), 5.36 (s, 2H) 4.39 (br s, 2H), 3.75 (s, 3H), 3.51 (br s, 2H), 3.24 (s, 2H). LCMS (MH+, 368.1).

*6-(4-Chloro-2-fluorobenzyl)-8,9,10,11-tetrahydropyrido-[4′,3′:4,5]thieno[3,2-e][1,2,4]triazolo[1,5-c]pyrimidin-5(6H)-one trifluoroacetate (**13**).* The title compound was prepared using general method B. ^{1}H NMR (400 MHz, DMSO-d_6) δ 9.19−9.35 (m, 2H), 8.57 (s, 1H), 7.54−7.59 (m, 1H), 7.42−7.51 (m, 1H), 7.23−7.30 (m, 1H), 5.45 (s, 2H), 4.38 (br s, 2H), 3.50 (br s, 2H), 3.23 (t, J = 5.46 Hz, 2H). LCMS (MH+, 390.1).

*6-(2-Fluoro-4-methoxybenzyl)-8,9,10,11-tetrahydropyrido-[4′,3′:4,5]thieno[3,2-e][1,2,4]triazolo[1,5-c]pyrimidin-5(6H)-one Trifluoroacetate (**14**).* The title compound was prepared using general method B. ^{1}H NMR (400 MHz, DMSO-d_6) δ 9.16−9.46 (br s, 2H), 8.56 (s, 1H), 7.34 (t, J = 8.85 Hz, 1H), 6.92 (dd, J = 12.42, 2.38 Hz, 1H), 6.76 (dd, J = 8.66, 2.38 Hz, 1H), 5.38 (s, 2H), 4.38 (s, 2H), 3.77 (s, 3H), 3.45−3.55 (m, 2H), 3.17−3.26 (m, 2H). LCMS (MH+, 386.1).

*11,11-Difluoro-6-(4-methoxybenzyl)-8,9,10,11-tetrahydropyrido-[4′,3′:4,5]thieno[3,2-e][1,2,4]triazolo[1,5-c]pyrimidin-5(6H)-one Hydrochloride (**15**).* Compound **9** (346 mg, 0.69 mmol) was diluted in 4N hydrochloric acid in dioxane (5.0 mL, 20 mmol), and the resulting solution was stirred at room temperature. After 4 h, the mixture was concentrated under reduced pressure and dried under vacuum to afford the hydrochloride salt of **15** as a yellow powder. ^{1}H NMR (400 MHz, DMSO-d_6) δ 8.56 (s, 1 H), 7.39 (d, J = 8.41 Hz, 2 H), 6.94 (d, J = 8.41 Hz, 2 H), 5.40 (s, 2 H), 4.49 (br s, 2 H), 4.05 (t, J = 11.42 Hz, 2 H), 3.75 (s, 3 H). LCMS (MH+, 404.1).

*6-(4-Chlorobenzyl)-9-methyl-8,9,10,11-tetrahydropyrido-[4′,3′:4,5]thieno[3,2-e][1,2,4]triazolo[1,5-c]pyrimidin-5(6H)-one (**16a**).* General method C: Triethylamine (0.034 mL, 0.24 mmol) was added to a mixture of **10** (100 mg, 0.24 mmol) in 1,2-dichloroethane (2 mL). After 5 min, aqueous formaldehyde (24 mg, 0.29 mmol) was

DOI: 10.1021/acs.jmedchem.7b00302
J. Med. Chem. XXXX, XXX, XXX−XXX

added and the resulting mixture was stirred for 1 h. Sodium triacetoxyborohydride (78 mg, 0.37 mmol) was added, and the resulting mixture was stirred for 4 h. The mixture was concentrated, diluted with DMF, filtered, and purified by reverse phase HPLC to afford the TFA salt of **16a**. This material was taken up in DCM, washed with sodium bicarbonate, dried ($MgSO_4$), and concentrated under vacuum to afford 11 mg (24%) of **16a** as an off-white solid. ^{1}H NMR (400 MHz, $CDCl_3$) δ 8.31 (s, 1H), 7.38−7.45 (m, 2H), 7.31−7.37 (m, 2H), 5.38 (s, 2H), 3.67 (s, 2H), 3.18−3.24 (m, 2H), 2.88 (t, J = 5.69 Hz, 2H), 2.56 (s, 3H). LCMS (MH+, 386.3). Anal. ($C_{18}H_{16}ClN_5OS$) C, H, N.

*6-(4-Chlorobenzyl)-9-(cyclopropylmethyl)-8,9,10,11-tetrahydropyrido[4′,3′:4,5]thieno[3,2-e][1,2,4]triazolo[1,5-c]-pyrimidin-5(6H)-one (**16b**).* The title compound was prepared using general method C. ^{1}H NMR (400 MHz, DMSO-d_6) δ 8.49 (s, 1H), 7.43 (d, J = 3.18 Hz, 4H), 5.37 (s, 2H), 3.68 (s, 2H), 2.97 (br s, 2H), 2.82−2.87 (m, 2H), 2.40 (d, J = 6.48 Hz, 2H), 0.83−0.96 (m, 1H), 0.49 (d, J = 7.58 Hz, 2H), 0.11 (d, J = 4.52 Hz, 2H). LCMS (MH+, 426.2). Anal. ($C_{21}H_{20}ClN_5OS$) C, H, N.

*6-(4-Chlorobenzyl)-9-(cyclopropanecarbonyl)-8,9,10,11-tetrahydropyrido[4′,3′:4,5]thieno[3,2-e][1,2,4]triazolo[1,5-c]-pyrimidin-5(6H)-one (**16c**).* Piperidine **10** (100 mg, 0.24 mmol), cyclopropanecarbonyl chloride (0.027 mL, 0.29 mmol), and triethylamine (0.10 mL, 0.73 mmol) were combined in DMA (2 mL) and stirred for 18 h. The mixture was filtered and purified by prep LCMS to afford 37 mg (34%) of **16c** as an off-white powder. ^{1}H NMR (400 MHz, DMSO-d_6) δ 8.51 (s, 1H), 7.39−7.50 (m, 4H), 5.38 (br s, 2H), 4.64−5.05 (m, 2H), 3.78−4.10 (m, 2H), 2.92−3.15 (m, 2H), 1.94−2.22 (m, 1H), 0.71−0.80 (m, 4H). LCMS (MH+, 440.2). Anal. ($C_{21}H_{18}ClN_5O_2S$) C, H, N.

*(RS)-9-(2,2-Difluorocyclopropanecarbonyl)-6-(4-methoxybenzyl)-8,9,10,11-tetrahydropyrido[4′,3′:4,5]thieno[3,2-e][1,2,4]triazolo[1,5-c]pyrimidin-5(6H)-one (**16d**).* Piperidine **12** (206 mg, 0.43 mmol), 2,2-difluorocyclopropanecarboxylic acid (64 mg, 0.47 mmol), dichloromethane (2 mL), triethylamine (0.066 mL, 0.47 mmol), and HOBt (72 mg, 0.47 mmol) were combined in that order and stirred for 15 min. EDCI (90 mg, 0.47 mmol) was added, and stirring was continued for 20 h. The mixture was diluted with DCM (10 mL) and then washed with saturated sodium bicarbonate solution. After filtering through a phase separating column, the solution was concentrated under vacuum and the residue was purified by flash LC (elution with 5−75% ethyl acetate in hexanes) to afford a white powder. This material was lyophilized from 1:1 dioxane−water to afford 27 mg (13%) of **16d** as a white powder. ^{1}H NMR (400 MHz, $CDCl_3$) δ 8.29 (s, 1H), 7.42 (d, J = 8.6 Hz, 2H), 6.88 (d, J = 8.6 Hz, 2H), 5.50−5.22 (m, 2H), 4.91−4.76 (m,2H), 4.06−3.88 (m, 2H), 3.80 (s, 3H), 3.71 (s, 2H), 3.28 (br s, 2H), 3.19 (br s, 1H), 2.69−2.53 (m,1H), 2.19 (dd, J = 5.0, 12.5 Hz, 1H), 1.80−1.65 (m, 1H). LCMS (MH+, 472.2). Anal. ($C_{22}H_{19}F_2N_5O_3S$) C, H, N.

*6-(4-Chlorobenzyl)-9-(oxetan-3-yl)-8,9,10,11-tetrahydropyrido-[4′,3′:4,5]thieno[3,2-e][1,2,4]triazolo[1,5-c]pyrimidin-5(6H)-one (**16e**).* The title compound was prepared using general method C. ^{1}H NMR (400 MHz, DMSO-d_6) δ 8.50 (s, 1H), 7.39−7.47 (m, 4H), 5.38 (s, 2H), 4.56−4.63 (m, 2H), 4.50 (t, J = 6.05 Hz, 2H), 3.68−3.77 (m, 1H), 3.56 (s, 2H), 2.95−3.03 (m, 2H), 2.69 (t, J = 5.32 Hz, 2H). LCMS (MH+, 428.1). Anal. ($C_{20}H_{18}ClN_5O_2S$) C, H, N.

*9-Benzyl-6-(4-chlorobenzyl)-8,9,10,11-tetrahydropyrido-[4′,3′:4,5]thieno[3,2-e][1,2,4]triazolo[1,5-c]pyrimidin-5(6H)-one (**16f**).* The title compound was prepared using general method C. ^{1}H NMR (400 MHz, $CDCl_3$) δ 8.30 (s, 1H), 7.50−7.42 (m, 6H), 7.41−7.35 (m, 2H), 7.35−7.30 (m,2H), 5.36 (br s, 2H), 4.39 (s, 4H), 3.57 (br s, 2H), 3.48 (br s, 2H). LCMS (MH+, 462.2). Anal. ($C_{24}H_{20}ClN_5OS$) C, H, N.

*6-(Benzyl)-9-((tetrahydro-2H-pyran-4-yl)methyl)-8,9,10,11-tetrahydropyrido[4′,3′:4,5]thieno[3,2-e][1,2,4]triazolo[1,5-c]-pyrimidin-5(6H)-one (**16g**).* The title compound was prepared using general method C. ^{1}H NMR (400 MHz, DMSO-d_6) δ 8.49 (s, 1H), 7.42−7.29 (m, 5H), 5.37 (s, 2H), 3.81 (dd, J = 2.6, 11.2 Hz, 2H), 3.60 (s, 2H), 3.30−3.22 (m, 2H), 2.97 (br s, 2H), 2.79 (t, J = 5.5 Hz, 2H), 2.39−2.31 (m, 2H), 1.82 (br s, 1H), 1.61 (d, J = 11.9 Hz, 2H), 1.19−1.05 (m, 2H). LCMS (MH+, 436.0). Anal. ($C_{23}H_{24}ClN_5O_2S$) C, H, N.

*6-(4-Chlorobenzyl)-9-((tetrahydro-2H-pyran-4-yl)methyl)-8,9,10,11-tetrahydropyrido[4′,3′:4,5]thieno[3,2-e][1,2,4]triazolo[1,5-c]pyrimidin-5(6H)-one (**16h**).* The title compound was prepared using general method C. ^{1}H NMR (400 MHz, $CDCl_3$) δ 8.32 (s, 1H), 7.40−7.45 (m, 2H), 7.33−7.38 (m, 2H), 5.39 (s, 2H), 4.00 (dd, J = 11.48, 2.95 Hz, 2H), 3.68 (s, 2H), 3.43 (td, J = 11.73, 1.76 Hz, 2H), 3.13−3.20 (m, 2H), 2.89 (t, J = 5.71 Hz, 2H), 2.46 (d, J = 7.15 Hz, 2H), 1.79−1.92 (m, 1H), 1.69−1.77 (m, 2H), 1.26−1.40 (m, 2H). LCMS (MH+, 470.2). Anal. ($C_{23}H_{24}ClN_5O_2S$) C, H, N.

*6-(4-Chloro-2-fluorobenzyl)-9-((tetrahydro-2H-pyran-4-yl)-methyl)-8,9,10,11-tetrahydropyrido[4′,3′:4,5]thieno[3,2-e][1,2,4]-triazolo[1,5-c]pyrimidin-5(6H)-one (**16i**).* The title compound was prepared using general method C. ^{1}H NMR (400 MHz, DMSO-d_6) δ 9.96 (br s, 1H), 8.58 (s,1 H), 7.53−7.61 (m, 1H), 7.43−7.52 (m, 1H), 7.25−7.32 (m, 1H), 5.35−5.58 (m, 2H), 4.69−4.85 (m, 1H), 4.30−4.46 (m, 1H), 3.76−3.93 (m, 4H), 3.33 (br s, 7H), 2.12 (br s, 1H), 1.67 (d, J = 14.68 Hz, 2H), 1.26 (qd, J = 12.05,4.14 Hz, 2H). LCMS (MH+, 488.1). Anal. ($C_{23}H_{23}ClFN_5O_2S$) C, H, N.

*6-(4-Methoxybenzyl)-9-((tetrahydro-2H-pyran-4-yl)methyl)-8,9,10,11-tetrahydropyrido[4′,3′:4,5]thieno[3,2-e][1,2,4]triazolo[1,5-c]pyrimidin-5(6H)-one (**16j**).* The title compound was prepared using general method C. ^{1}H NMR (400 MHz, DMSO-d_6) δ 8.48 (s, 1H), 7.35−7.33 (m, 2H), 6.91−6.89 (m, 2H), 5.29 (s, 2H), 3.81 (dd, J = 9.0, 2.1 Hz, 2H), 3.72 (s, 3H), 3.60 (br s, 1H), 3.28 (t, J = 9.2 Hz, 2H), 2.95−2.94 (m, 2H), 2.78−2.76 (m, 2H), 2.34 (d, J = 5.8 Hz, 2H), 1.82−1.81 (m, 1H), 1.62−1.59 (m, 2H), 1.12 (qd, J = 10.1, 3.1 Hz, 2H). LCMS (MH+, 466.2). Anal. ($C_{24}H_{27}N_5O_3S$) C, H, N.

*6-(2-Fluoro-4-methoxybenzyl)-9-((tetrahydro-2H-pyran-4-yl)-methyl)-8,9,10,11-tetrahydropyrido[4′,3′:4,5]thieno[3,2-e][1,2,4]-triazolo[1,5-c]pyrimidin-5(6H)-one (**16k**).* The title compound was prepared using general method C. ^{1}H NMR (400 MHz, DMSO-d_6) δ 8.50 (s, 1H), 7.30 (t, J = 8.85 Hz, 1H), 6.90 (dd, J = 12.49, 2.32 Hz, 1H), 6.74 (dd, J = 8.60, 2.32 Hz, 1H), 5.34 (s, 2H), 3.80−3.87 (m, 2H), 3.62 (s, 2H) 3.77 (s, 3H), 3.24−3.31 (m, 2H), 2.93−3.02 (m, 2H), 2.76−2.84 (m, 2H), 2.33−2.40 (m, 2H), 1.76−1.91 (m, 1H), 1.57−1.68 (m, 2H), 1.07−1.22 (m, 2H). ^{13}C NMR (101 MHz, $CDCl_3$) δ 161.31 (d, J = 11.0 Hz), 161.42 (d, J = 247 Hz), 154.47, 149.65, 145.12, 144.83, 130.55 (d, J = 5.1 Hz), 129.32, 127.58, 112.48 (d, J = 14.7 Hz), 110.65 (d, J = 2.9 Hz), 110.07, 101.67 (d, J = 25.7 Hz), 67.85, 63.54, 55.65, 51.66, 49.85, 44.92 (d, J = 3.7 Hz), 33.11, 31.62, 25.19. LCMS (MH+, 484.2). Anal. ($C_{24}H_{26}FN_5O_3S$) C, H, N.

*11,11-Difluoro-6-(4-methoxybenzyl)-9-((tetrahydro-2H-pyran-4-yl)methyl)-8,9,10,11-tetrahydropyrido[4′,3′:4,5]thieno[3,2-e][1,2,4]-triazolo[1,5-c]pyrimidin-5(6H)-one (**17**).* The title compound was prepared using general method C. ^{1}H NMR (400 MHz, $CDCl_3$) δ 8.42 (s, 1H), 7.41 (d, J = 8.66 Hz, 2H), 6.91 (d, J = 8.66 Hz, 2H), 5.40 (s, 2H), 3.96−4.04 (m, 2H), 3.82 (s, 5H), 3.38−3.47 (m, 2H), 3.28 (t, J = 11.54 Hz, 2H), 2.58 (d, J = 7.28 Hz, 2H), 1.80−1.94 (m, 1H), 1.69−1.78 (m, 2H), 1.25−1.39 (m, 2H). ^{13}C NMR (101 MHz, $CDCl_3$) δ 160.07, 154.89, 148.47, 145.83, 144.77, 136.13 (t, J = 8.8 Hz), 129.87, 125.08 (t, J = 30.8 Hz), 124.97, 114.82 (t, J = 241 Hz), 114.44, 107.53, 67.71, 62.22, 58.32 (t, J = 28.6 Hz), 55.34, 51.80, 51.40, 32.95, 31.24. LCMS (MH+, 502.2). Anal. ($C_{24}H_{25}F_2N_5O_3S$) C, H, N.

PDE Inhibition. PDE1B inhibition IC_{50} values were determined by an IMAP assay measuring inhibition of FAM-cAMP hydrolysis by full length PDE1 enzymes. Specifically, in 1536-well white plates, 250 pg per well of GST tagged PDE1B was dispensed in 2.5 μL of IMAP assay buffer consisting of 10 mM Tris pH 7.2, 10 mM $MgCl_2$, 1 mM DTT, 0.1% fatty acid free BSA, with 10 U/mL calmodulin, and 2.5 mM $CaCl_2$. Then 30 nL of compound was added from 1 mM stock in DMSO using the Kalypsys 1536 pintool. Plates were incubated for 5 min at room temperature before dispensing 1.5 μL of 533 nM FAM-cAMP for a final concentration of 200 nM. The plates were incubated 30 min at room temperature after a brief centrifugation. The assay was terminated by adding 5 μL of IMAP binding reagent Tb complex to each well, prepared according to manufacturer's recommendations. Plates were incubated 1 h at room temperature and read on the Viewlux. PDE2A, PDE3A, PDE4D, and PDE10A values were determined using analogous procedures. PDE5A, PDE6C, PDE7A,

DOI: 10.1021/acs.jmedchem.7b00302
J. Med. Chem. XXXX, XXX, XXX−XXX

PDE8A, PDE9A, and PDE11A values were determined at BPS Bioscience.

Protein Expression, Purification, Crystallization, and Crystal Handling. A polyhistidine-tag−tobacco etch virus (TEV) protease cleavage site sequence followed by the bacterial codon optimized cDNA corresponding to human PDE1B1 (UniProt entry Q01064-1) residues 146−506 and PDE10A1 (UniProt entry Q9Y233-1) residues 439−779 were subcloned into separate pNIC28-Bsa4 expression vectors. The pNIC28-Bsa4 was a gift from Opher Gileadi (Addgene plasmid no. 26103).[38] The resulting plasmids were transformed into the *Escherichia coli* Rosetta 2 (DE3) strain (EMD Millipore). Cultures grown in Terrific Broth medium were induced with 0.1 and 0.5 mM isopropyl β-D-thiogalactopyranoside (IPTG) at OD600 = 3.0 for PDE1B and PDE10A, respectively. At the time of induction, the incubation temperature was lowered to 18 °C. The cells were harvested 16 h post induction.

Following cell lysis, the PDE1B protein was affinity purified with Ni-NTA resin. Following TEV protease treatment, and concurrent dialysis, the protein was passed over a bed of Ni-NTA resin. The flow-through was concentrated and injected onto a HiLoad 16/600 Superdex 200 column equilibrated with 10 mM Tris, 100 mM NaCl, and 1 mM TCEP, pH 8.0. The elution peak corresponding to the target protein was concentrated to 11 mg/mL. The protein was incubated with 200 μM BAY 60-7550 and crystallized by the hanging drop vapor diffusion method at 20 °C with a well solution containing 100 mM HEPES pH 6.9 and 3.1 M NaCl.[39] Compound **3** and **16j** were introduced by soaking crystals overnight in solutions matching the well solution but with 25% glycerol and 2.5 mM compound. Crystals were mounted in cryo loops and flash-frozen in liquid nitrogen.

The PDE10A protein was purified as previously described.[40] The purified protein in 20 mM HEPES, 150 mM NaCl, 5 mM DTT, pH 7.5, was concentrated to 15 mg/mL. Apo crystals of human PDE10A were obtained by the hanging drop vapor diffusion method at 20 °C with a well solution containing 15% PEG3350, 200 mM calcium acetate, and 10 mM 2-mercaptoethanol. Crystals were first soaked in well solution containing 1 mM 3-isobutyl-1-methylxanthine (IBMX) overnight. Compound **16d** was introduced through a second soaking step by transferring the IBMX soaked crystals to a solution matching the well solution supplied with 5 mM of compound **16d**. After 24 h, crystals were washed with a cryo solution (75% well solution plus 25% ethylene glycol) and flash-frozen in liquid nitrogen.

Structure Determination. Single-crystal X-ray diffraction data were collected at cryogenic temperature (100 K). The PDE1B data were collected at beamline 5.0.2 at the Advanced Light Source, Lawrence Berkeley National Laboratory (Berkeley, CA) and processed with DIALS.[41] The PDE10A data were collected at the Stanford Synchrotron Radiation Lightsource (SSRL), SLAC National Accelerator Laboratory (Menlo Park, CA) and processed with XDS.[42] The initial phases were generated by molecular replacement using publically available PDE1B and PDE10A catalytic domain structures (PDBs 1TAZ and 5C2H, respectively).[26,43] The structures were built with COOT and refined with Phenix.[44,45] The X-ray data processing and structure refinement statistics are reported in Supporting Information, Table S1. Figures were generated with PyMOL.[46] Only chain A of the PDE10A−**16d** cocomplex structure was used for ligand binding analysis. In chain B, the ligand conformation is influenced by crystal packing (Supporting Information, Figure S2).

Metabolic Stability in the Presence of Liver Microsomes. Test compound was incubated at a final concentration of 1 μM in a reaction mixture containing human or rat liver microsomes of 0.5 mg protein/mL in Tris buffer at 37 °C. The reaction was started by addition of NADPH (1 μM). Aliquots of the incubation mixture were removed and quenched with three volumes of cold ACN containing internal standard, indomethacin (0.5 μM) at 0, 5, 15, and 30 min for RLM and at 0, 15, 30, and 60 min for HLM. The samples were vortex mixed and centrifuged at 4000 rpm for 10 min at 40 °C, and the supernatant was transferred to a 384-well plate followed by dilution with same volume of distilled water. Then 5 μL of the samples were analyzed using a Shimadzu HPLC system (Kyoto, Japan) equipped with a reversed-phase column (Thermo Hypersil GOLD 3 μm drop-in guard cartridges, 10 mm × 2.1 mm). Mobile phase was consisted of 0.1% formic acid in water and of 0.1% formic acid in ACN with a flow rate of 0.7 mL/min. Eluent was directed to an API4000 triple quadruple mass spectrometer (AB Sciex, Framingham, MA) equipped with a turbo electrospray interface. Multiple reaction monitoring (MRM) transition in positive ion mode was used. Integration of the sample peaks was performed using AB Sciex Analyst and DiscoveryQuant software; peak area ratio of the analyte to the internal standard was determined accordingly. In vitro intrinsic clearance (CL_{int}) was calculated by dividing the first-order degradation rate constant (K_{deg}) by the concentration of microsomal protein used in the incubation. K_{deg} was the slope using least-squares fit to the curve of percent test compound remaining vs time (0−30 min for RLM and 0−60 min for HLM).

Rat Pharmacokinetics Determination. Pharmacokinetics properties in male SD rats (300−350g) were determined following intravenous (IV) and oral (PO) administration. For IV dosing (N = 3, 1 mg/kg), rats were catheterized in jugular and femoral vein. For PO dosing (N = 3, 5 mg/kg), rats were catheterized in femoral vein. Test article was formulated in NMP:PEG400:water (10:40:50). Rats were not fasted during this study. Blood was sampled at 0 (predose), 0.033, 0.083, 0.25, 0.5, 1, 2, 4, 8, 12, 16, and 24 h following IV and at 0 (predose), 0.25, 0.5, 1, 2, 4, 8, 12, 16, and 24 h following PO dosing. Plasma was isolated by centrifugation, and all samples were frozen at −80 °C. Calibration standards were prepared by the addition of known concentrations of test article to blank rat plasma to provide a calibration range of 0.5−2000 ng/mL. Then 50 μL plasma samples or calibration standard was added to 250 μL of internal standard solution in acetonitrile. Samples were vortex mixed and centrifuged at 12000 rpm for 5 min at 4 °C. Supernatant (100 μL) was transferred to labeled autosampler vials containing 300 μL of mobile phase (water/acetonitrile/formic acid, 90/10/0.2%), vortex mixed, and analyzed by LC-MS/MS. A bioanalytical method was developed for the quantification of test article in rat plasma. Method development and sample analysis was conducted using a Waters Quattro Premier LC-MS/MS system equipped with Waters Acquity UPLC system. Then 5 μL of the samples were analyzed using a Waters Acquity UPLC system equipped with a C 18 reversed-phase column (Phenomenex Kinetex C18, 1.7 μm, 2.1 mm × 50.0 mm). Mobile phase consisted of 0.1% formic acid in water and of 0.1% formic acid in acetonitrile with a flow rate of 0.7 mL/min. Eluent was directed to a Waters Quattro Premier mass spectrometer equipped with a turbo electrospray interface. Multiple reaction monitoring (MRM) transition in positive ion mode was used.

For CNS penetration studies male SD rats (300−350 g) were dosed PO (N = 3, 10 mg/kg). Test article was formulated in NMP:PEG400:-water (10:40:50). Animals were anesthetized, and approximately 0.3 mL of blood from each rat was collected via cardiac puncture into tubes containing lithium heparin as the anticoagulant at 1 h post dose. Plasma was isolated by centrifugation. Animals were then decapitated and brains were removed. All samples were stored frozen at approximately −80 °C until analysis. Plasma analysis was performed as described above.

One hemisphere of each brain sample was weighed. One to five dilutions (w/v) were prepared by addition of 1:1 mixture of water/2-propanol (4-fold of the brain weight) to each brain sample. Brains were homogenized by Fast Prep Calibration standards (ranging from 0.500 to 2000 ng/mL), quality control samples, and test samples containing the internal standard (IS) were separated from rat brain preparations via protein precipitation by addition of 100 μL of 75:25 acetonitrile/water solvent containing analyte calibrants and 300 μL of acetonitrile/IS solution mix (40 ng/mL in acetonitrile) to 100 μL brain homogenate. Following vortex mixing and centrifugation, 20 μL aliquots of the supernatants were diluted with 580 μL of 20:80 acetonitrile/water containing 0.2% formic acid and mixed for the 10 mg/kg study. Following vortex mixing and centrifugation, 100 μL aliquots of the supernatants were diluted with 300 μL of 10:90 acetonitrile/water containing 0.2% formic acid and mixed for the 1.0 mg/kg study.

DOI: 10.1021/acs.jmedchem.7b00302
J. Med. Chem. XXXX, XXX, XXX−XXX

Then 5 μL of each sample was applied to a Kinetex 1.7 μm C18, 100 Å, 50 mm × 2.1 mm column (Phenomenex, Torrance, CA) and eluted with a mobile phase gradient (initial 10% B hold for 0.1 min, then 10% B to 90% B in 1.0 min) consisting of solution A (0.1% formic acid in water) and solution B (0.1% formic acid in acetonitrile). The column temperature was maintained at 30 °C. The column eluent was subjected to positive-mode electrospray ionization (ES+), and the analytes were detected with a QTrap 5500 quadrupole/ion trap mass spectrometer (AB Sciex, Framingham, MA).

Novel Object Recognition Training and Testing. Rats were handled for three days and habituated to the testing arena for 10 min. On training day, drug was administered orally in a vehicle of 10% DMSO, 30% PEG 400, and 60% saline at a volume of 2 mL/kg. Animals were then placed into the training box and allowed to explore two identical objects for either 3 min (to induce a weak memory) or for 15 min (to induce a strong memory). Memory retention was tested for 5 min 24 h after training. Animals were presented with one "familiar" (training) and one "novel" object. Objects were placed into the central area of the box, and the spatial position of objects (left–right sides) was counterbalanced between subjects. After each experimental subject, the apparatus and the objects were thoroughly cleaned with 90% ethanol, dried, and ventilated for a few minutes. To determine memory, an object-discrimination index (DI) was determined as [novel exploration − familiar exploration]/ [total exploration], which is shown as the memory score (DI × 100). In addition, the time exploring the objects during training was recorded. Data were analyzed by least-squares means planned comparisons, the results of which are presented. All data are presented as the mean ± SEM.

■ ASSOCIATED CONTENT

Supporting Information

The Supporting Information is available free of charge on the ACS Publications website at DOI: 10.1021/acs.jmedchem.7b00302.

Crystal packing in **16j**/PDE1B and **16d**/PDE10A, X-ray data processing and structure refinement statistics, off-target selectivity data for **16k**(PDF)

Molecular formula strings (CSV)

Accession Codes

The crystal structures of **3** in PDE1B (5UP0), **16d** in PDE10A (5UWF), and **16j** in PDE1B (5UOY) were deposited with the RCSB PDB. Authors will release the atomic coordinates and experimental data upon article publication.

■ AUTHOR INFORMATION

Corresponding Author

*Phone: 858-736-3044. E-mail: bdyck@dartneuroscience.com.

ORCID

Brian Dyck: 0000-0001-5225-8706

Laurent Gomez: 0000-0002-9172-7840

Notes

The authors declare no competing financial interest.

■ ACKNOWLEDGMENTS

The Berkeley Center for Structural Biology is supported in part by the National Institutes of Health, National Institute of General Medical Sciences, and the Howard Hughes Medical Institute. The Advanced Light Source is supported by the Director, Office of Science, Office of Basic Energy Sciences, of the U.S. Department of Energy under Contract No. DE-AC02-05CH11231. Use of the Stanford Synchrotron Radiation Lightsource, SLAC National Accelerator Laboratory, is supported by the U.S. Department of Energy, Office of Science, Office of Basic Energy Sciences under Contract No. DE-AC02-76SF00515. The SSRL Structural Molecular Biology Program is supported by the DOE Office of Biological and Environmental Research and by the National Institutes of Health, National Institute of General Medical Sciences (including P41GM103393). The contents of this publication are solely the responsibility of the authors and do not necessarily represent the official views of NIGMS or NIH. We thank Kristen Arienti for proof reading the manuscript and Grace Yan for additional pharmacological experiments.

■ ABBREVIATIONS USED

br s, broad signal; CREB, CAMP-response element binding protein; DIEA, diisopropylethylamine; EDC, 1-ethyl-3-(3-(dimethylamino)propyl)carbodiimide; FAM-CAMP, FAM-cAMP, 2′-(6-[fluoresceneinyl] aminohexylcarbamoyl)-adenosine-3′,5′-cyclic monophosphate; HLM, human liver microsomes; IMAP, immobilized metal ion affinity-based fluorescence polarization; HOBt, 1-hydroxybenzotriazole; MDCK, Madin–Darby canine kidney; NOR, novel object recognition; RLM, rat liver microsomes

■ REFERENCES

(1) Mattson, M. P.; Chan, S. L.; Duan, W. Modification of brain aging and neurodegenerative disorders by genes, diet, and behavior. *Physiol. Rev.* **2002**, *82*, 637–672.

(2) Millan, M. J.; Agid, Y.; Brüne, M.; Bullmore, E. T.; Carter, C. S.; Clayton, N. S.; Connor, N.; Davis, S.; Deakin, B.; DeRubeis, R. J.; Dubois, B.; Geyer, M. A.; Goodwin, G. M.; Gorwood, P.; Jay, T. M.; Joëls, M.; Mansuy, I. M.; Meyer-Lindenberg, A.; Murphy, D.; Rolls, E.; Saletu, B.; Spedding, M.; Sweeney, J.; Whittington, M.; Young, L. J. Cognitive dysfunction in psychiatric disorders: characteristics, causes and the quest for improved therapy. *Nat. Rev. Drug Discovery* **2012**, *11*, 141–168.

(3) Esposito, K.; Reierson, G. W.; Luo, H. R.; Wu, G. S.; Licinio, J.; Wong, M. L. Phosphodiesterase genes and antidepressant treatment response: a review. *Ann. Med.* **2009**, *41*, 177–185.

(4) Conti, M.; Beavo, J. A. Biochemistry and physiology of cyclic nucleotide phosphodiesterases: essential components in cyclic nucleotide signaling. *Annu. Rev. Biochem.* **2007**, *76*, 481–511.

(5) Lugnier, C. Cyclic nucleotide phosphodiesterase (PDE) superfamily: A new target for the development of specific therapeutic agents. *Pharmacol. Ther.* **2006**, *109*, 366–398.

(6) Schmidt, C. J. Phosphodiesterase inhibitors as potential cognition enhancing agents. *Curr. Top. Med. Chem.* **2010**, *10*, 222–230.

(7) Menniti, F. S.; Faraci, W. S.; Schmidt, C. J. Phosphodiesterases in the CNS: targets for drug development. *Nat. Rev. Drug Discovery* **2006**, *5*, 660–670.

(8) Bitner, R. S. Cyclic AMP response element-binding protein (CREB) phosphorylation: a mechanistic marker in the development of memory enhancing Alzheimer's disease therapeutics. *Biochem. Pharmacol.* **2012**, *83*, 705–714.

(9) Lu, Y. F.; Kandel, E. R.; Hawkins, R. D. Nitric oxide signaling contributes to late-phase LTP and CREB phosphorylation in the hippocampus. *J. Neurosci.* **1999**, *19*, 10250–10261.

(10) Bliss, T. V.; Collingridge, G. L. A synaptic model of memory: long-term potentiation in the hippocampus. *Nature* **1993**, *361*, 31–39.

(11) Frey, U.; Huang, Y. Y.; Kandel, E. R. Effects of cAMP simulate a late stage of LTP in hippocampal CA1 neurons. *Science* **1993**, *260*, 1661–1664.

(12) Reed, T. M.; Repask, D. R.; Snyder, G. L.; Greengard, P.; Vorhees, C. V. Phosphodiesterase 1B knock-out mice exhibit exaggerated locomotor hyperactivity and DARPP-32 phosphorylation in response to dopamine agonists and display impaired spatial learning. *J. Neurosci.* **2002**, *22*, 5188–5197.

DOI: 10.1021/acs.jmedchem.7b00302
J. Med. Chem. XXXX, XXX, XXX–XXX

(13) Medina, A. E. Therapeutic utility of phosphodiesterase type I inhibitors in neurological conditions. *Front. Neurosci.* **2011**, *5*, 21.
(14) Rossato, J. I.; Bevilaqua, L. R. M.; Izquierdo, I.; Medina, J. H.; Cammarota, M. Dopamine controls persistence of long-term memory storage. *Science* **2009**, *325*, 1017−1020.
(15) Nishi, A.; Kuroiwa, M.; Shuto, T. Mechanisms for the modulation of dopamine D1 receptor signaling in striatal neurons. *Front. Neuroanat.* **2011**, *5*, 43.
(16) (a) Wennogle, L. P. *PDE1 Inhibitors for Cognitive Dysfunction in Schizophrenia*; Biochemical Pharmacology Discussion Group, New York Academy of Sciences: New York, January 26, 2010. (b) Li, P.; Zheng, H.; Zhao, J.; Zhang, L.; Yao, W.; Zhu, H.; Beard, J. D.; Ida, K.; Lane, W.; Snell, G.; Sogabe, S.; Heyser, C. J.; Snyder, G. L.; Hendrick, J. P.; Vanover, K. E.; Davis, R. E.; Wennogle, L. P. Discovery of potent and selective inhibitors of phosphodiesterase 1 for the treatment of cognitive impairment associated with neurodegenerative and neuropsychiatric diseases. *J. Med. Chem.* **2016**, *59*, 1149−1164. (c) Snyder, G. L.; Prickaerts, J.; Wadenberg, M. L.; Zhang, L.; Zheng, H.; Yao, W.; Akkerman, S.; Zhu, H.; Hendrick, J. P.; Vanover, K. E.; Davis, R.; Li, P.; Mates, S.; Wennogle, L. P. Preclinical profile of ITI-214, an inhibitor of phosphodiesterase 1, for enhancement of memory performance in rats. *Psychopharmacology* **2016**, *233*, 3113−3124.
(17) Hindmarch, I.; Fuchs, H.-H.; Erzigkeit, H. Efficacy and tolerance of vinpocetine in ambulant patients suffering from mild to moderate organic psychosyndromes. *Int. Clin. Psychopharmacol.* **1991**, *6*, 31−44.
(18) Xia, Y.; Chackalamannil, S.; Czarniecki, M.; Tsai, H.; Vaccaro, H.; Cleven, R.; Cook, J.; Fawzi, A.; Watkins, R.; Zhang, H. Synthesis and evaluation of polycyclic pyrazol[3,4-d]pyrimidines as PDE1 and PDE5 cGMP phosphodiesterase inhibitors. *J. Med. Chem.* **1997**, *40*, 4372−4377.
(19) Ahn, H. S.; Bercovici, A.; Boykow, G.; Bronnenkant, A.; Chackalamannil, S.; Chow, J.; Cleven, R.; Cook, J.; Czarniecki, M.; Domalski, C.; Fawzi, A.; Green, M.; Gundes, A.; Ho, G.; Laudicina, M.; Lindo, N.; Ma, K.; Manna, M.; McKittrick, B.; Mirzai, B.; Nechuta, T.; Neustadt, B.; Puchalski, C.; Pula, K.; Silverman, L.; Smith, E.; Stamford, A.; Tedesco, R. P.; Tsai, H.; Tulshian, D.; Vaccaro, H.; Watkins, R. W.; Weng, X.; Witkowski, J. T.; Xia, Y.; Zhang, H. Potent tetracyclic guanine inhibitors of PDE1 and PDE5 cyclic guanosine monophosphate phosphodiesterases with oral antihypertensive activity. *J. Med. Chem.* **1997**, *40*, 2196−2210.
(20) Verhoest, P. R.; Proulx-Lafrance, C.; Corman, M.; Chenard, L.; Helal, C. J.; Hou, X.; Kleiman, R.; Liu, S.; Marr, E.; Menniti, F. S.; Schmidt, C. J.; Vanase-Frawley, M.; Schmidt, A. W.; Williams, R. D.; Nelson, F. R.; Fonseca, K. R.; Liras, S. Identification of a brain penetrant PDE9A inhibitor utilizing prospective design and chemical enablement as a rapid lead optimization strategy. *J. Med. Chem.* **2009**, *52*, 7946−7949.
(21) Verhoest, P. R.; Fonseca, K. R.; Hou, X.; Proulx-Lafrance, C.; Corman, M.; Helal, C. J.; Claffey, M. M.; Tuttle, J. B.; Coffman, K. J.; Liu, S.; Nelson, F.; Kleiman, R. J.; Menniti, F. S.; Schmidt, C. J.; Vanase-Frawley, M.; Liras, S. Design and discovery of 6[(3*S*,4*S*)4-methyl-1-(pyrimidin-2-ylmethyl)pyrrolidin-3-yl]-1-(tetrahydro-*H*-pyran-4-yl)-1,5-dihydro-4*H*-pyrazolo[3,4-*d*]pyrimidin-4-one (PF-04447943), a selective brain penetrant PDE9A inhibitor for the treatment of cognitive disorders. *J. Med. Chem.* **2012**, *55*, 9045−9054.
(22) Claffey, M. M.; Helal, C. J.; Verhoest, P. R.; Kang, Z.; Fors, K. S.; Jung, S.; Zhong, J.; Bundesmann, M. W.; Hou, X.; Lui, S.; Kleiman, R. J.; Vanase-Frawley, M.; Schmidt, A. W.; Menniti, F.; Schmidt, C. J.; Hoffman, W. E.; Hajos, M.; McDowell, L.; O'Connor, R. E.; MacDougall-Murphy, M.; Fonseca, K. R.; Becker, S. L.; Nelson, F. R.; Liras, S. Application of structure-based drug design and parallel chemistry to identify selective, brain penetrant, in vivo active phosphodiesterase 9A inhibitors. *J. Med. Chem.* **2012**, *55*, 9055−9068.
(23) Vemulapalli, S.; Watkins, R. W.; Chintala, M.; Davis, H.; Ahn, H.-S.; Fawzi, A.; Tulshian, D.; Chiu, P.; Chatterjee, M.; Lin, C.-C.; Sybertz, E. Antiplatelet, and antiproliferative effects of SCH 51866, a novel type 1 and type 5 phosphodiesterase inhibitor. *J. Cardiovasc. Pharmacol.* **1996**, *28*, 862−869.
(24) *PDE Inhibitor Platform*; Intra-Cellular Therapies: New York, 2014; http://www.intracellulartherapies.com/products-technology/pde-inhibitor-platform.html (accessed March 20, 2017).
(25) Humphrey, J. M.; Yang, E.; am Ende, C. W.; Arnold, E. P.; Head, J. L.; Jenkinson, S.; Lebel, L. A.; Liras, S.; Pandit, J.; Samas, B.; Vajdos, F.; Simons, S. P.; Evdokimov, A.; Mansour, M.; Menniti, F. S. Small-molecule phosphodiesterase probes: discovery of potent and selective CNS-penetrable quinazoline inhibitors of PDE1. *MedChemComm* **2014**, *5*, 1290−1296.
(26) Zhang, K. Y.; Card, G. L.; Suzuki, Y.; Artis, D. R.; Fong, D.; Gillette, S.; Hsieh, D.; Neiman, J.; West, B. L.; Zhang, C.; Milburn, M. V.; Kim, S. H.; Schlessinger, J.; Bollag, G. A glutamine switch mechanism for nucleotide selectivity by phosphodiesterases. *Mol. Cell* **2004**, *15*, 279−286.
(27) Wang, T.; Huang, X.-G.; Liu, J.; Li, B.; Wu, J.-J.; Chen, K.-X.; Zhu, W.-L.; Xu, X.-Y.; Zeng, B.-B. An efficient one-pot synthesis of substituted 2-aminothiophenes via three-component Gewald reaction catalyzed by L-proline. *Synlett* **2010**, *2010*, 1351−1354.
(28) Thorn, A.; Zinner, G. Bifunktionelle elektrophile zur darstellung [c]-heteroanellierter chinazolinon-derivate: 2-isocyanatocyclohex-1-encarbonsäurenitril, ergänzend zu 2-isocyanatobenzonitril. *Arch. Pharm.* **1994**, *327*, 469−475.
(29) Cote, R. H. Characteristics of photoreceptor PDE (PDE6): similarities and differences to PDE5. *Int. J. Impotence Res.* **2004**, *16*, S28−S33.
(30) Ennaceur, A.; Delacour, J. A new one-trial test for neurobiological studies of memory in rats. 1: behavioral data. *Behav. Brain Res.* **1988**, *31*, 47−59.
(31) Teng, E.; Stefanacci, L.; Squire, L. R.; Zola, S. M. Contrasting effects on discrimination learning after hippocampal lesions and conjoint hippocampal-caudate lesions in monkeys. *J. Neurosci.* **2000**, *20*, 3853−3863.
(32) Zola, S. M.; Squire, L. R.; Teng, E.; Stefanacci, L.; Buffalo, E. A.; Clark, R. E. Impaired recognition memory in monkeys after damage limited to the hippocampal region. *J. Neurosci.* **2000**, *20*, 451−463.
(33) Mumby, D. G. Perspectives on object-recognition memory following hippocampal damage: lessons from studies in rats. *Behav. Brain Res.* **2001**, *127*, 159−181.
(34) Barker, G. R.; Warburton, E. C. When is the hippocampus involved in recognition memory? *J. Neurosci.* **2011**, *31*, 10721−10731.
(35) Ennaceur, A.; Neave, N.; Aggleton, J. P. Spontaneous object recognition and object location memory in rats: the effects of lesions in the cingulate cortices, the medial prefrontal cortex, the cingulum bundle and the fornix. *Exp. Brain Res.* **1997**, *113*, 509−519.
(36) Viosca, J.; Malleret, G.; Bourtchouladze, R.; Benito, E.; Vronskava, S.; Kandel, E. R.; Barco, A. Chronic enhancement of CREB activity in the hippocampus interferes with retrieval of spatial information. *Learn. Mem.* **2009**, *16*, 198−209.
(37) Allan, A.; Branstetter, B.; Breitenbucher, J.; Dyck, B.; Gharbaoui, T.; Gomez, L.; Hudson, A. R.; Marrone, T. J.; Vickers, T.; Weinhouse, M. I. Therapeutic thiophene-, furan-, and pyridine-fused azolopyrimidin-5-(6*H*)-ones. US 2013/0338139 Al, 2013.
(38) Savitsky, P.; Bray, J.; Cooper, C. D.; Marsden, B. D.; Mahajan, P.; Burgess-Brown, N. A.; Gileadi, O. High-throughput production of human proteins for crystallization: the SGC experience. *J. Struct. Biol.* **2010**, *172*, 3−13.
(39) Boess, F. G.; Hendrix, M.; van der Staay, F. J.; Erb, C.; Schreiber, R.; van Staveren, W.; de Vente, J.; Prickaerts, J.; Blokland, A.; Koenig, G. Inhibition of phosphodiesterase 2 increases neuronal cGMP, synaptic plasticity and memory performance. *Neuropharmacology* **2004**, *47*, 1081−1092.
(40) Recht, M. I.; Sridhar, V.; Badger, J.; Bounaud, P. Y.; Logan, C.; Chie-Leon, B.; Nienaber, V.; Torres, F. E. Identification and optimization of PDE10A inhibitors using fragment-based screening by nanocalorimetry and X-ray crystallography. *J. Biomol. Screening* **2014**, *19*, 497−507.
(41) Waterman, D. G.; Winter, G.; Parkhurst, J. M.; Fuentes-Montero, L.; Hattne, J.; Brewster, A. S.; Sauter, N. K.; Evans, G. The

DOI: 10.1021/acs.jmedchem.7b00302
J. Med. Chem. XXXX, XXX, XXX−XXX

DIALS framework for integration software. *CCP4 Newsl. Protein Crystallogr.* **2013**, *49*, 16−19.
(42) Kabsch, W. XDS. *Acta Crystallogr., Sect. D: Biol. Crystallogr.* **2010**, *66*, 125−132.
(43) Shipe, W. D.; Sharik, S. S.; Barrow, J. C.; McGaughey, G. B.; Theberge, C. R.; Uslaner, J. M.; Yan, Y.; Renger, J. J.; Smith, S. M.; Coleman, P. J.; Cox, C. D. Discovery and optimization of a series of pyrimidine-based phosphodiesterase 10A (PDE10A) inhibitors through fragment screening, structure-based design, and parallel synthesis. *J. Med. Chem.* **2015**, *58*, 7888−7894.
(44) Emsley, P.; Lohkamp, B.; Scott, W. G.; Cowtan, K. Features and development of *Coot*. *Acta Crystallogr., Sect. D: Biol. Crystallogr.* **2010**, *66*, 486−501.
(45) Adams, P. D.; Afonine, P. V.; Bunkoczi, G.; Chen, V. B.; Davis, I. W.; Echols, N.; Headd, J. J.; Hung, L. W.; Kapral, G. J.; Grosse-Kunstleve, R. W.; McCoy, A. J.; Moriarty, N. W.; Oeffner, R.; Read, R. J.; Richardson, D. C.; Richardson, J. S.; Terwilliger, T. C.; Zwart, P. H. *PHENIX*: a comprehensive Python-based system for macromolecular structure solution. *Acta Crystallogr., Sect. D: Biol. Crystallogr.* **2010**, *66*, 213−221.
(46) *The PyMOL Molecular Graphics System*, version 1.7.6.4; Schrödinger, LLC.

DOI: 10.1021/acs.jmedchem.7b00302
J. Med. Chem. XXXX, XXX, XXX−XXX